[redacted] ~~CONFIDENTIAL~~

SEP 5 - 1957

Copy
RM L5[illegible]

TECH LIBRARY KAFB, NM

0144784

NACA RM L57G12

7795

RESEARCH MEMORANDUM

EFFECTS OF WING WARP ON THE LIFT, DRAG, AND STATIC LONGITUDINAL STABILITY CHARACTERISTICS OF AN AIRCRAFT CONFIGURATION HAVING AN ARROW WING OF ASPECT RATIO 1.86 AT MACH NUMBERS FROM 1.1 TO 1.7

By Warren Gillespie, Jr.

Langley Aeronautical Laboratory
Langley Field, Va.

[redacted]

NATIONAL ADVISORY COMMITTEE
FOR AERONAUTICS

WASHINGTON
August 30, 1957

~~CONFIDENTIAL~~

[redacted]

TECH LIBRARY KAFB, N.Y.
0144784

NATIONAL ADVISORY COMMITTEE FOR AERONAUTICS

RESEARCH MEMORANDUM

EFFECTS OF WING WARP ON THE LIFT, DRAG, AND STATIC LONGITUDINAL STABILITY CHARACTERISTICS OF AN AIRCRAFT CONFIGURATION HAVING AN ARROW WING OF ASPECT RATIO 1.86 AT MACH NUMBERS FROM 1.1 TO 1.7

By Warren Gillespie, Jr.

SUMMARY

The results of a free-flight investigation to determine the effect of wing warp on the lift, drag, and static longitudinal stability characteristics of a low-drag aircraft configuration employing an arrow wing of aspect ratio 1.86 are presented. The mean surface shape of the warped wing was derived from a lifting surface theory for a design lift coefficient of 0.2 at a Mach number of 1.57. Data from a similar plane-wing model provided a basis for comparison. Lift, drag, and pitching-moment coefficients were obtained at Mach numbers from 1.1 to 1.7, and at Reynolds numbers from 5×10^6 to 11×10^6 per foot of length.

Wing warp reduced the axial-force and total drag coefficients above a lift coefficient of 0.2. The maximum lift-drag ratios of the warped-wing model were 10 to 4 percent higher than those of the plane-wing model. However the maximum ratios of lift coefficient raised to the one-half power divided by the corresponding drag coefficient were 8 to 9 percent lower for the warped-wing model.

INTRODUCTION

Two methods of wing design appear capable of improving the performance of supersonic aircraft. Results obtained to date by the method of wing warp (refs. 1 to 6) indicate that this method is effective up to low supersonic speeds and design lift coefficients less than 0.3. The results obtained by the method of inboard chord extension (refs. 7 to 10) indicate that both range and maximum speed can be increased at the higher

[redacted]

supersonic Mach numbers (at least to a Mach number of 2) for which the method of wing warp becomes ineffective. The warped-wing models that have been tested (except that of ref. 6) have been designed for Mach numbers below 1.3. At such Mach numbers the vortex drag contributes most to the drag due to lift, and is effectively reduced by the simpler method of conical camber (ref. 1). At somewhat higher supersonic Mach numbers the compound warp method (refs. 11 and 12) should be the more effective warp method in reducing the combined vortex and wave drag due to lift.

The purpose of the present investigation is to determine experimentally whether any benefits can be realized by employing the compound warp method at a design Mach number of 1.57 and a wing design lift coefficient of 0.2 on a low-drag aircraft configuration having an arrow wing of aspect ratio 1.86 and a leading-edge sweep of 67.5°. At this design condition reference 11 was used to determine the wing twist and camber. The model was flight tested at Mach numbers of 1.1 to 1.7 from the Langley Pilotless Aircraft Research Station at Wallops Island, Va.

SYMBOLS

C_N normal-force coefficient, $\frac{a_n}{g}\frac{W/S}{q}$

C_X axial-force coefficient, $\frac{a_x}{g}\frac{W/S}{q}$

C_L lift coefficient, $C_N \cos\alpha + C_X \sin\alpha$

C_D drag coefficient, $-C_X \cos\alpha + C_N \sin\alpha$

L/D lift-drag ratio

C_m pitching-moment coefficient about model center of gravity, $\frac{I_Y\ddot{\theta}}{qS\bar{c}}$

$C_{N_\alpha} = \left(\frac{\partial C_N}{\partial \alpha}\right)_{C_N=0}$

$C_{m_{C_N}}$ static stability parameter in pitch, $\left(\frac{\partial C_m}{\partial C_N}\right)_{C_N=0}$

[redacted]

c_l	local lift coefficient based on local chord, $\frac{\text{Lift per unit span}}{qc}$
c_l'	local lift coefficient based on local span, $\frac{\text{Lift per unit chord}}{2qy}$
P	lifting pressure coefficient
a_n	normal acceleration, ft/sec^2
a_x	longitudinal acceleration, ft/sec^2
g	acceleration due to gravity, 32.2 ft/sec^2
q	dynamic pressure, lb/sq ft
M	Mach number
R	Reynolds number based on a length of 1 foot
α	angle of attack, deg
β	angle of sideslip, deg
$\ddot{\theta}$	angular acceleration in pitch, radians/sec^2
p	rolling velocity, radians/sec
x, y, z	rectangular coordinates
$\sigma \equiv \frac{2y}{b}$	
b	total wing span, 2.83 ft
$\bar{c}$	wing mean aerodynamic chord, 2.03 ft
c	local wing chord, ft
c_r	wing root chord, 3.04 ft
S	total wing area to body center line, 4.31 sq ft

W weight of model, 107.0 lb

I_Y model moment of inertia in pitch about center of gravity, 10.89 slug-ft^2

MODEL

A drawing of the model is shown in figure 1 and photographs are presented in figure 2. The fuselage ordinates are listed in table I, and physical characteristics of the model are listed in table II. The configuration of this investigation was the same as that of reference 13 except that the mean surface shape of the wing was derived from the lifting-surface theory of reference 11 for a design lift coefficient of 0.2 at a Mach number of 1.57. The model had an arrow wing of aspect ratio 1.86 with a leading-edge sweep of 67.5° and NACA 65A004 airfoil-section thickness distribution about the mean camber line. The fuselage was a body of fineness ratio 20. A triangular vertical tail with 60° leading-edge sweep and NACA 65A003 airfoil section provided directional stability.

The side-view photographs in figure 2 indicate the warped-wing contour. The wing ordinates are given in table III. A contour diagram and the loadings used in the design method are shown in figures 3 and 4. The one straight-line wing element was located at the trailing edge for convenience. The angle of incidence of the wing with the body was selected to give zero lift for zero angle of attack of the body center line.

The model was of metal with a solid aluminum-alloy wing. Four pulse rockets and a telemeter with angle-of-attack, angle-of-sideslip, accelerometer, and roll-rate instrumentation were carried in the model, which was externally boosted by two Deacon rockets. An underslung adapter was used to couple the model and booster. A support fitting, shown in figure 1, extended below the fuselage and remained with the model.

PROCEDURE

A wing panel was statically tested to measure the streamwise wing twist due to loading concentrated along the 50-percent-chord line. The flexibility was found to be essentially the same as that reported in reference 13 for the plane-wing model; however, a slight increase in stiffness due to wing warp was noted.

The model was flight tested at Mach numbers of 1.1 to 1.7 from the Langley Pilotless Aircraft Research Station at Wallops Island, Va. Data were obtained during ascent of the model after separation from the rocket booster. Aerodynamic data were obtained from transient oscillations induced by the pulse rockets, which fired at intervals in the pitch direction. The telemeter system permitted the measurement of angles of attack and sideslip, normal and longitudinal accelerations, angular pitch acceleration, and rolling velocity. The flight velocity obtained from a CW Doppler radar set (corrected for wind velocity) was used in conjunction with tracking radar and radiosonde data to calculate Mach number, Reynolds number, and dynamic pressure. The variations of the free-stream Reynolds number and dynamic pressure with Mach number are shown in figure 5.

ACCURACY AND CORRECTIONS

Errors in the absolute value of a telemetered quantity are thought to be within ±1 percent of the range of the instrument. At a Mach number of 1.5 the errors in the normal- and axial-force coefficients have been estimated to be within ±0.02, and ±0.001, respectively. Mach number is estimated to be accurate within ±1 percent and dynamic pressure within ±2 percent. Experience in the use of the air-flow indicator shows that an error of $\pm 0.3^{\circ}$ is probable.

An additional source of inaccuracy in the final results may be the induced lateral motions following a pitch pulse. However, cross-coupling effects on the data presented are believed to be small.

Measurements obtained from the flow indicator were corrected for pitching velocity and for flight-path curvature. Measurements obtained from the normal and longitudinal accelerometers were corrected to values at the model center of gravity. Wing aeroelastic corrections to the data were not made. Such corrections would be small. For example, there is an estimated reduction of C_{N_α} from rigid-wing values of only 4 percent.

RESULTS AND DISCUSSION

The aerodynamic test results are presented in figures 6 to 13. Since the stiffness of the warped wing was almost the same as that of the plane wing, and the test conditions were similar, the data of this investigation are directly comparable with the data for the plane-wing model (ref. 13) for determination of the effects of wing warp.

Trim

Figure 6 presents trim measurements for the model. The model has a favorable trim angle of attack of approximately 1.7° as a result of the wing warp. However, since the model rolled steadily at a rate of approximately 4 radians per second, the trim angles of attack and yaw for zero roll rate could be somewhat less than these measured values. The higher trim roll rate for the warped-wing model, compared with a roll rate of less than 1 radian per second for the plane-wing model, is believed to be caused by slight wing asymmetries arising from the increased difficulty of accurately machining the warped-wing panels.

Drag

Axial-force and drag polars were obtained at Mach numbers of 1.11, 1.31, 1.54, and 1.74, and are shown in figures 7 and 8, respectively. The axial-force data of figure 7 indicate a reduction in axial-force coefficient with increasing normal-force coefficient. Compared with plane-wing values, there is a reduction in axial-force coefficient above a normal-force coefficient of 0.20 and, as seen in figure 8, a reduction in drag coefficient above a lift coefficient of 0.17, approximately. The drag at zero lift was increased approximately 50 percent by the wing warp.

Lift-Drag Ratios

Figure 9 presents L/D and $\frac{C_L^{1/2}}{C_D}$ both plotted against lift coefficient at Mach numbers of 1.11, 1.31, 1.54, and 1.74, for increasing and decreasing values. Maximum lift-drag ratios from 8.3 to 7.0 occurred at lift coefficients from 0.25 to 0.2. Maximum values from 17.7 to 16.6 occurred in $\frac{C_L^{1/2}}{C_D}$ at lift coefficients from 0.17 to 0.14. The variations of these maximum ratios and optimum lift coefficients with Mach number are shown in figure 10. Comparison is made with corresponding values for the plane wing. The maximum lift-drag ratios of the warped-wing model were 10 to 4 percent higher (with increase in Mach number) than those of the plane wing. However the maximum values of $\frac{C_L^{1/2}}{C_D}$ were 8 to 9 percent lower for the warped-wing model. The use of the amount of wing warp $(C_L = 0.2)$ of this investigation may or may not increase the maximum supersonic range of a turbojet-powered aircraft. This is so because for such an airframe-engine combination the optimum flight attitude of the airframe $(L/D)_{max}$ is compromised by the optimum operating conditions

of the powerplant. Depending upon the extent of supersonic Mach number effects on turbojet engine performance, the turbojet-powered aircraft may or may not operate near $(L/D)_{max}$ or $\frac{C_L^{1/2}}{C_D}$ for maximum flight range. The optimum lift coefficients for the warped-wing configuration are higher than those for the plane-wing configuration.

Normal Force and Pitching Moment

Figures 11 to 13 present plots of normal-force and pitching-moment coefficients and summarize the variations of the normal-force-curve and pitching-moment-curve slopes with Mach number. Figure 11 shows that the variation of normal-force coefficient with angle of attack is essentially linear for small angles of attack. The variation of normal-force coefficient with pitching-moment coefficient presented in figure 12 is also essentially linear over the range of test conditions. The variation of the normal-force-curve slope C_{N_α} with Mach number shown in figure 13(a) is similar to that for the plane-wing model but the curve is approximately 10 percent higher for the warped-wing case. The variation of the static-stability parameter $C_{m_{C_N}}$ with Mach number (fig. 13(b)) shows that the aerodynamic-center location was not changed by wing warp. The aerodynamic-center location was approximately constant with change in Mach number.

CONCLUDING REMARKS

A free-flight investigation of the effect of wing camber and twist on the supersonic lift, drag, and static longitudinal stability characteristics of a rocket-powered model having a 67.5° swept arrow wing of aspect ratio 1.86 and no horizontal-tail surface leads to the following observations:

1. Wing warp reduced the axial-force coefficient above a normal-force coefficient of 0.20 and the drag coefficient above a lift coefficient of 0.17 but increased the drag at zero lift by approximately 50 percent.

2. The maximum lift-drag ratios of the warped-wing configuration were 10 to 4 percent greater than the values for the plane-wing

configuration. However, the maximum values of $\frac{C_L^{1/2}}{C_D}$ were 8 to 9 percent lower for the warped-wing case.

Langley Aeronautical Laboratory,
National Advisory Committee for Aeronautics,
Langley Field, Va., June 21, 1957.

REFERENCES

1. Boyd, John W., Migotsky, Eugene, and Wetzel, Benton E.: A Study of Conical Camber for Triangular and Sweptback Wings. NACA RM A55G19, 1955.

2. Burrows, Dale L., and Tucker, Warren A.: A Transonic Wind-Tunnel Investigation of the Static Longitudinal Characteristics of a 3-Percent-Thick, Aspect-Ratio-3, Delta Wing Cambered and Twisted for High Lift-Drag Ratios. NACA RM L55F02a, 1955.

3. Saltzman, Edwin J., Bellman, Donald R., and Musialowski, Norman T.: Flight-Determined Transonic Lift and Drag Characteristics of the YF-102 Airplane With Two Wing Configurations. NACA RM H56E08, 1956.

4. Peterson, Victor L., and Boyd, John W.: Effects of Conical Camber on the Lift, Drag, and Pitching-Moment Characteristics of a Triangular Wing of Aspect Ratio 3.0. NACA RM A56L18, 1957.

5. Phelps, E. Ray, and Boyd, John W.: A Wind-Tunnel Investigation of the Effects of Conical Camber for an Airplane Configuration Having a Triangular Wing of Aspect Ratio 2.2. NACA RM A57A10, 1957.

6. Gillespie, Warren, Jr.: Effect of Wing Camber and Twist at Mach Numbers From 1.4 to 2.1 on the Lift, Drag, and Longitudinal Stability of a Rocket-Powered Model Having a 52.5° Sweptback Wing of Aspect Ratio 3 and Inline Tail Surfaces. NACA RM L56C16, 1956.

7. Sevier, John R., Jr.: Effects of a Series of Inboard Plan-Form Modifications on the Longitudinal Characteristics of Two Unswept Wings of Aspect Ratio 3.5, Taper Ratio 0.2, and Different Thickness Distributions at Mach Numbers of 1.61 and 2.01. NACA RM L53K11, 1954.

8. Cooper, Morton, and Sevier, John R., Jr.: Effects of a Series of Inboard Plan-Form Modifications on the Longitudinal Characteristics of Two 47° Sweptback Wings of Aspect Ratio 3.5, Taper Ratio 0.2, and Different Thickness Distributions at Mach Numbers of 1.61 and 2.01. NACA RM L53E07a, 1953.

9. Sevier, John R., Jr.: Investigation of the Effects of Body Indentation and of Wing-Plan-Form Modification on the Longitudinal Characteristics of a 60° Swept-Wing—Body Combination at Mach Numbers of 1.41, 1.61, and 2.01. NACA RM L55E17, 1955.

10. Henning, Allen B.: Effects of Wing Inboard Plan-Form Modifications on Lift, Drag, and Longitudinal Stability at Mach Numbers From 1.0 to 2.3 of a Rocket-Propelled Free-Flight Model With a 52.5° Sweptback Wing of Aspect Ratio 3. NACA RM L57D29, 1957.

11. Tucker, Warren A.: A Method for the Design of Sweptback Wings Warped to Produce Specified Flight Characteristics at Supersonic Speeds. NACA Rep. 1226, 1955. (Supersedes NACA RM L51F08.)

12. Grant, Frederick C.: The Proper Combination of Lift Loadings for Least Drag on a Supersonic Wing. NACA Rep. 1275, 1956. (Supersedes NACA TN 3533.)

13. Gillespie, Warren, Jr.: Supersonic Aerodynamic Characteristics of a Low-Drag Aircraft Configuration Having an Arrow Wing of Aspect Ratio 1.86 and a Body of Fineness Ratio 20. NACA RM L57A25, 1957.

TABLE I.- FUSELAGE ORDINATES

Station, in.	Body radius, in.
0	0
.67	.22
1.33	.38
1.67	.44
2.33	.57
3.33	.73
5.00	.98
6.67	1.19
10.00	1.54
13.33	1.82
16.67	2.06
20.00	2.23
22.75	2.35
23.33	2.37
26.67	2.45
30.00	2.50
Constant radius	Constant radius
63.38	2.50
67.43	2.45
71.49	2.37
75.54	2.23
79.60	2.06
83.65	1.82
87.71	1.54
91.76	1.19
93.79	.98
95.82	.73
97.04	.57
97.85	.44
98.25	.38
99.06	.21
99.87	0

TABLE II.- CHARACTERISTICS OF MODEL

Wing:	
Span, ft	2.83
Area, sq ft	4.31
Aspect ratio	1.86
Taper ratio	0
Sweepback of leading edge, deg	67.5
Sweepback of trailing edge, deg	15.0
Mean aerodynamic chord, $\bar{c}$, ft	2.03
Airfoil section thickness distribution	NACA 65A004
Design lift coefficient	0.20
Design Mach number	1.57
Body:	
Maximum diameter, ft	0.42
Length, ft	8.32
Fineness ratio	20
Vertical tail:	
Span, ft	0.97
Taper ratio	0
Sweepback of leading edge, deg	60
Sweepback of trailing edge, deg	15
Airfoil section	NACA 65A003
Model weight, lb	107.0
Moment of inertia in pitch, slug-ft^2	10.89
Center of gravity, percent $\bar{c}$ behind leading edge of mean aerodynamic chord	24.3

[redacted]

TABLE III.- WING ORDINATES MEASURED FROM REFERENCE

PLANE 0.44 INCH BELOW MODEL CENTER LINE

σ = 0.30			σ = 0.40			σ = 0.60			σ = 0.80		
x, in.	y_L, in.	y_U, in.	x, in.	y_L, in.	y_U, in.	x, in.	y_L, in.	y_U, in.	x, in.	y_L, in.	y_U, in.
0	-0.58	-0.58	0	-0.75	-0.75	0	-0.89	-0.89	0	-0.80	-0.80
1.55	-.46	.02	.90	-.70	-.39	.60	-.82	-.64	.30	-.75	-.68
2.75	-.40	.24	1.90	-.62	-.13	1.30	-.73	-.45	.70	-.69	-.57
3.95	-.36	.39	2.90	-.56	.04	2.00	-.67	-.30	1.00	-.64	-.49
5.15	-.34	.50	3.90	-.52	.17	2.70	-.61	-.19	1.40	-.59	-.39
6.35	-.33	.57	4.90	-.48	.27	3.40	-.57	-.09	1.70	-.55	-.33
7.55	-.34	.61	5.90	-.46	.35	4.10	-.53	-.01	2.10	-.51	-.27
8.75	-.36	.63	6.90	-.44	.40	4.80	-.49	.06	2.40	-.48	-.22
9.95	-.38	.64	7.90	-.43	.43	5.50	-.46	.12	2.80	-.44	-.17
11.15	-.39	.63	8.90	-.41	.44	6.20	-.42	.15	3.10	-.41	-.13
12.35	-.40	.61	9.90	-.40	.45	6.90	-.38	.17	3.50	-.37	-.09
13.55	-.39	.57	10.90	-.39	.44	7.60	-.35	.18	3.80	-.33	-.06
14.75	-.38	.52	11.90	-.37	.42	8.30	-.32	.19	4.20	-.29	-.04
15.95	-.38	.47	12.90	-.36	.40	9.00	-.28	.19	4.50	-.26	-.02
17.15	-.36	.42	13.90	-.34	.37	9.70	-.25	.18	4.90	-.22	-.01
18.35	-.33	.35	14.90	-.31	.33	10.40	-.22	.17	5.20	-.19	0
19.55	-.29	.28	15.90	-.27	.28	11.10	-.18	.14	5.60	-.15	.01
20.75	-.24	.21	16.90	-.24	.24	11.80	-.15	.12	5.90	-.12	.02
21.95	-.19	.16	17.90	-.20	.19	12.50	-.10	.09	6.30	-.08	.02
23.15	-.14	.10	18.90	-.16	.14	13.20	-.07	.06	6.60	-.06	.01
24.35	-.07	.05	19.90	-.11	.09	13.90	-.03	.03	7.00	-.02	.01
25.55	0	0	20.90	-.05	.05	14.60	0	0	7.30	0	0
			21.90	0	0						
L.E. radius = 0.03			L.E. radius = 0.02			L.E. radius = 0.02			L.E. radius = 0.01		

[redacted]

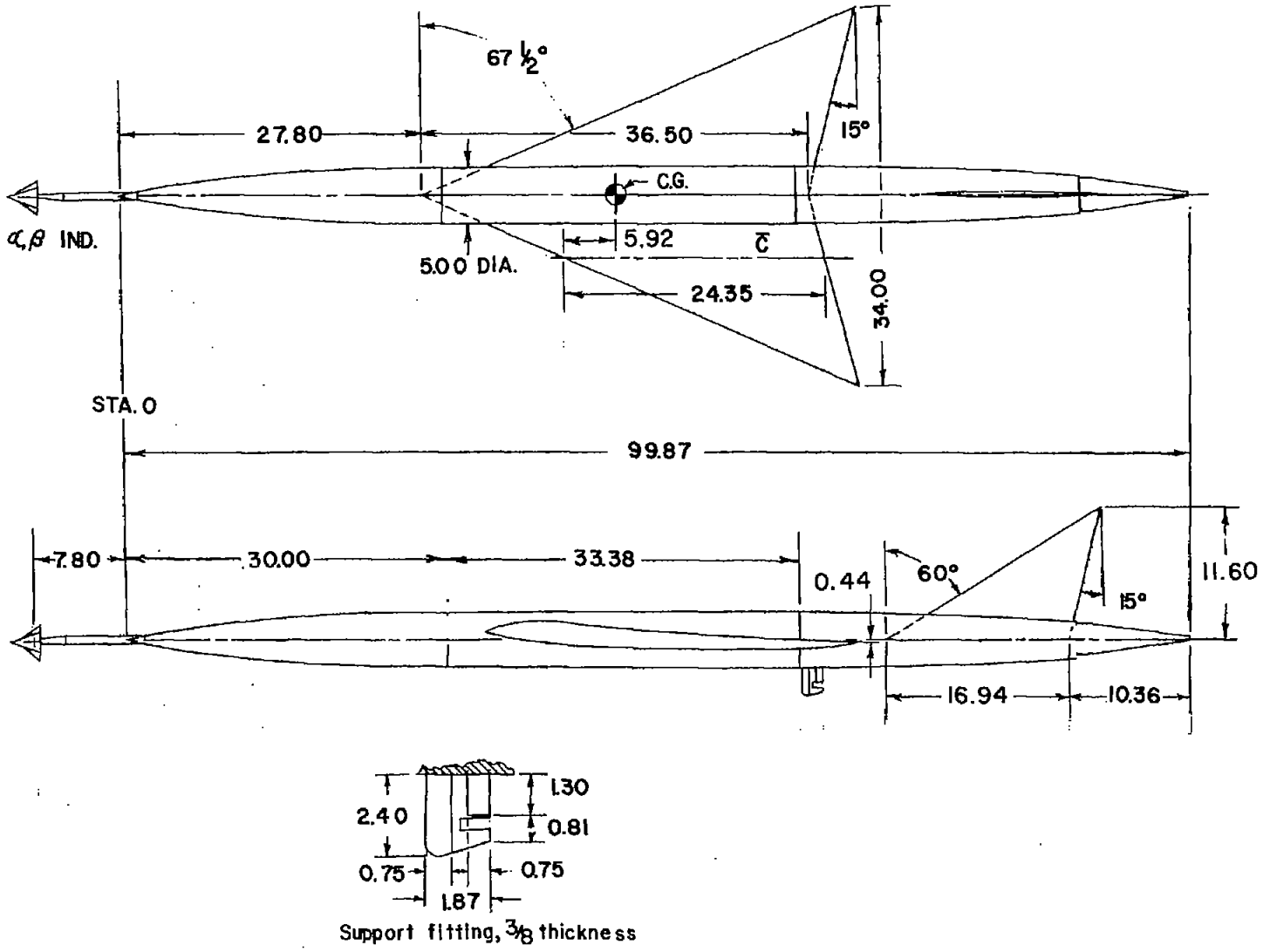

Figure 1.- Test configuration. All linear dimensions are in inches.

CONFIDENTIAL

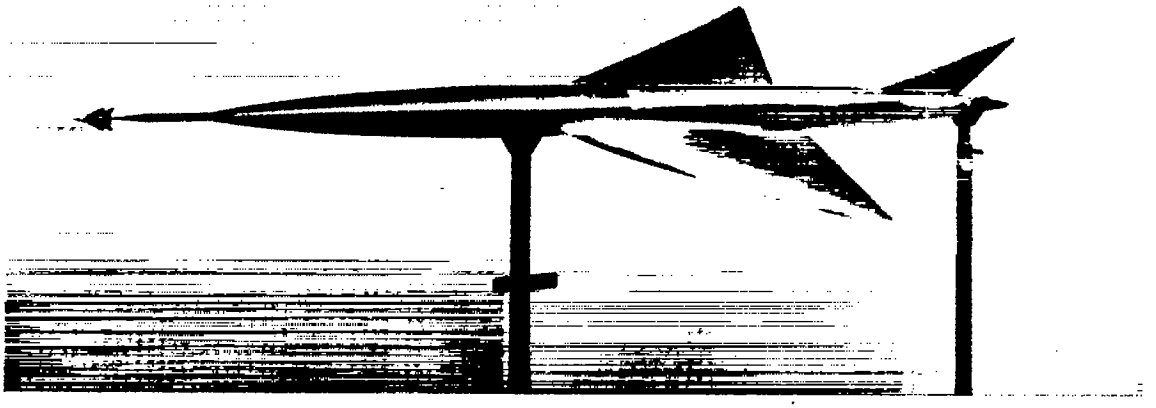

(a) Three-quarter front view.

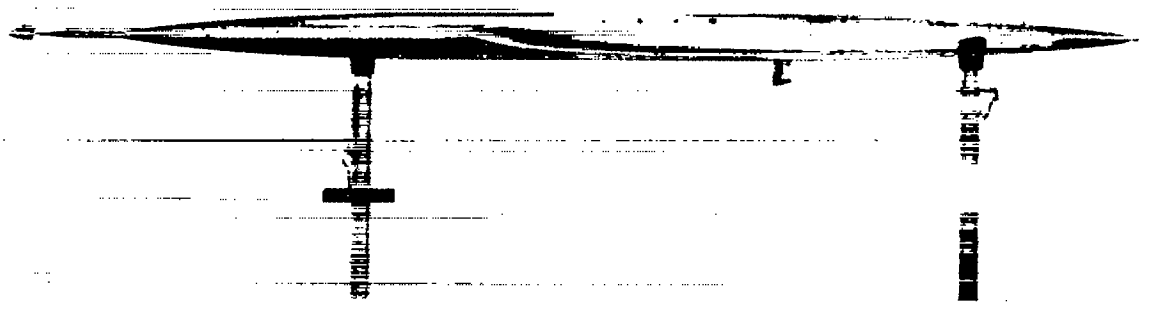

(b) Side view. L-57-1642

Figure 2.- Photographs of model with warped wing.

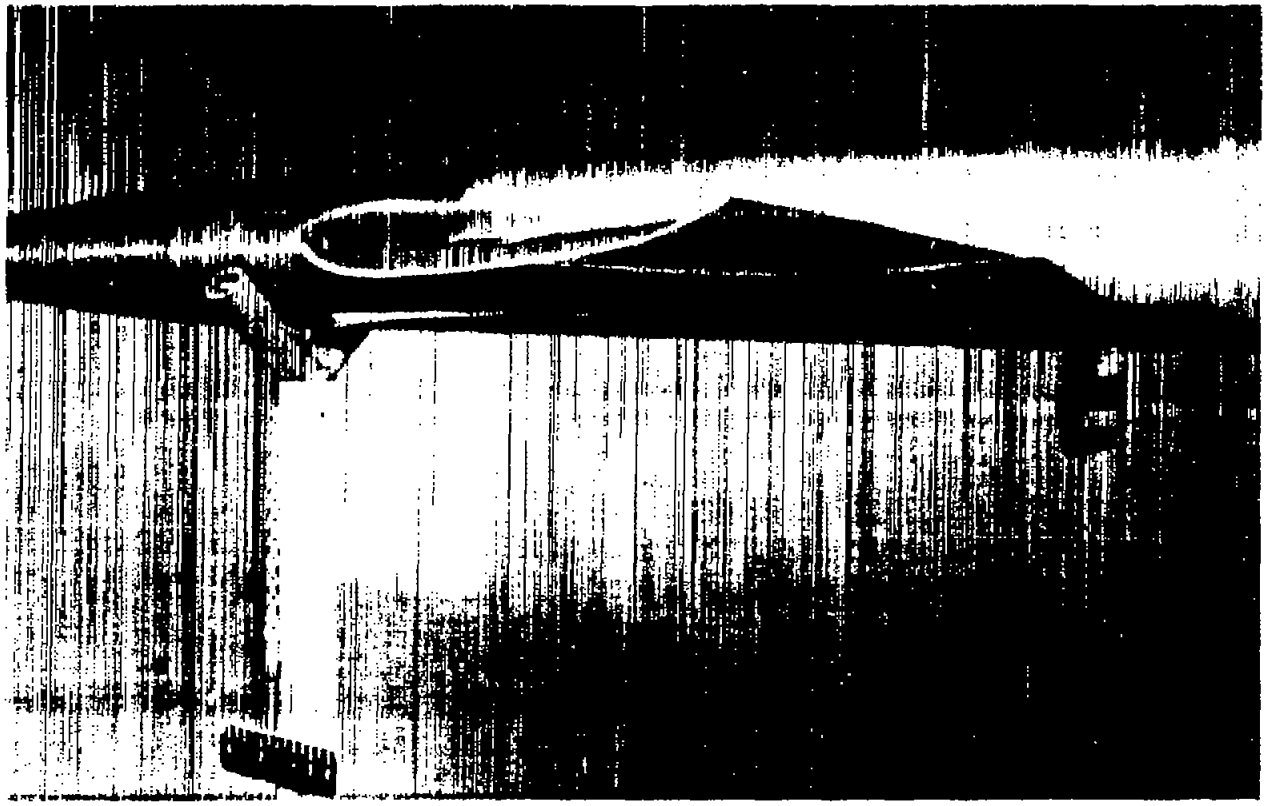

(c) Closeup showing warped wing panel. L-91342

Figure 2.- Concluded.

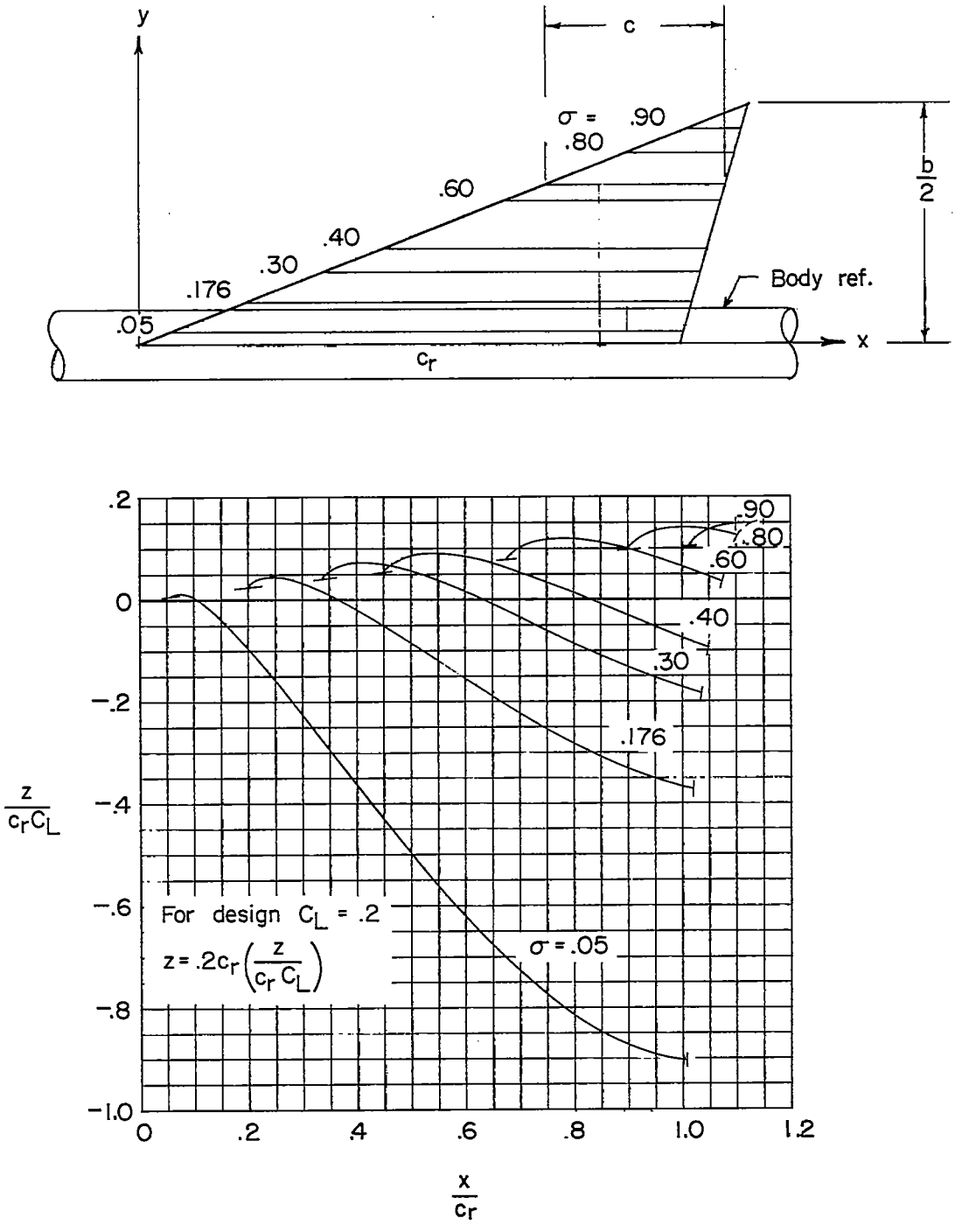

Figure 3.- Calculated wing warp for a Mach number of 1.57.

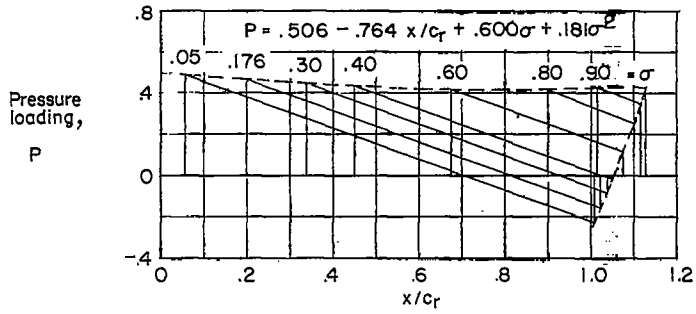

(a) Pressure loading.

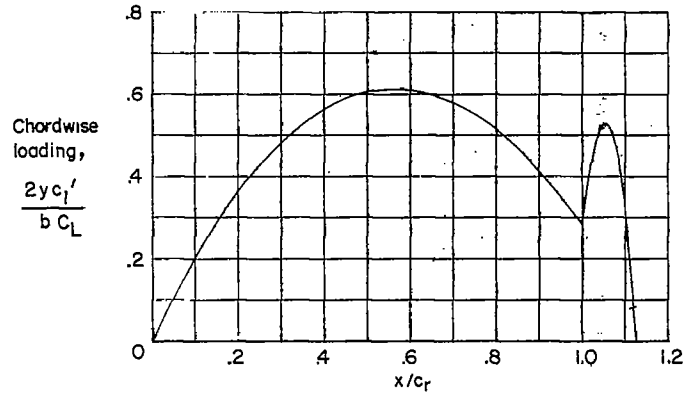

(b) Chordwise loading.

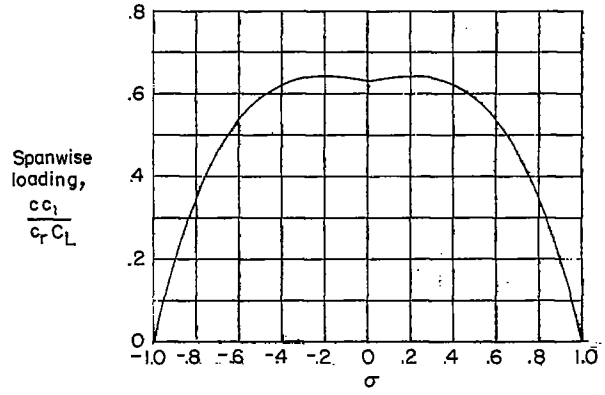

(c) Spanwise loading.

Figure 4.- Calculated loading distributions at a design lift coefficient of 0.2 and a Mach number of 1.57.

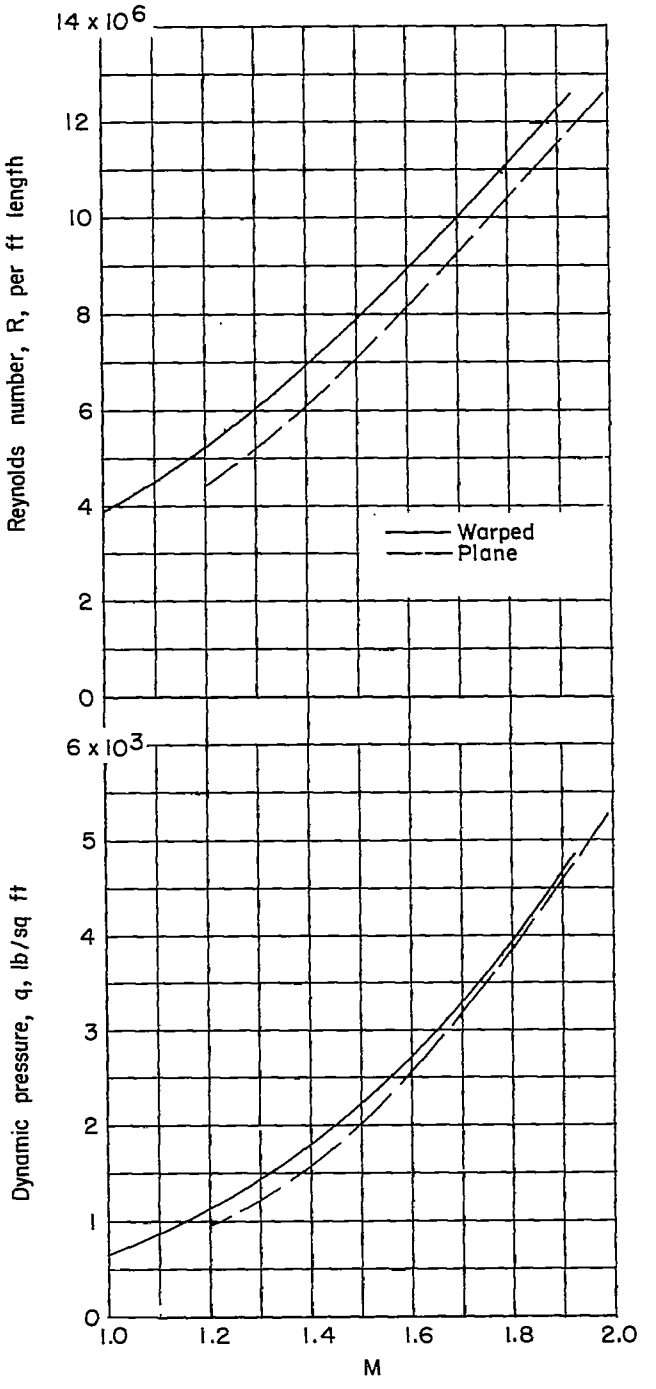

Figure 5.- Flight-test conditions.

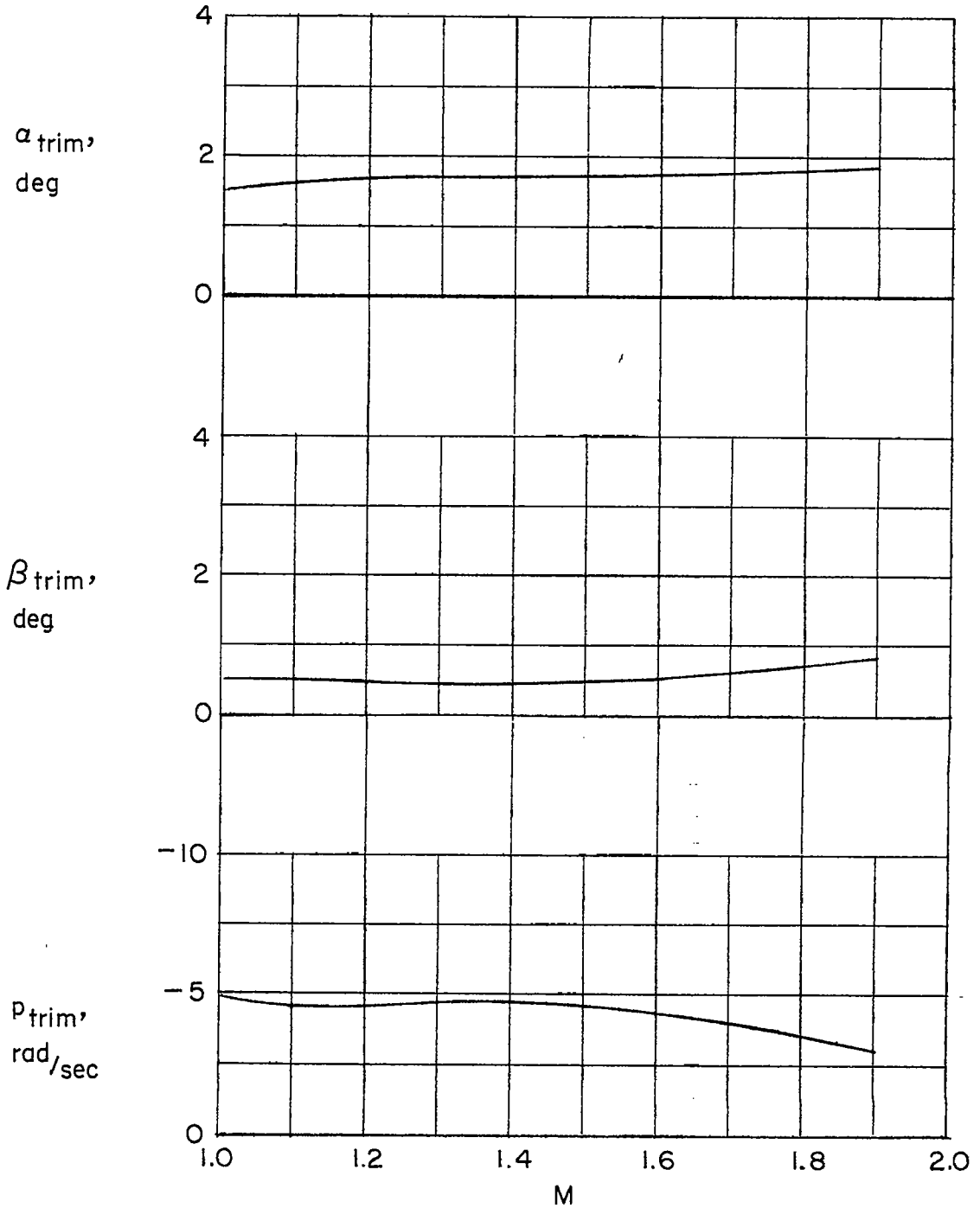

Figure 6.- Model trim.

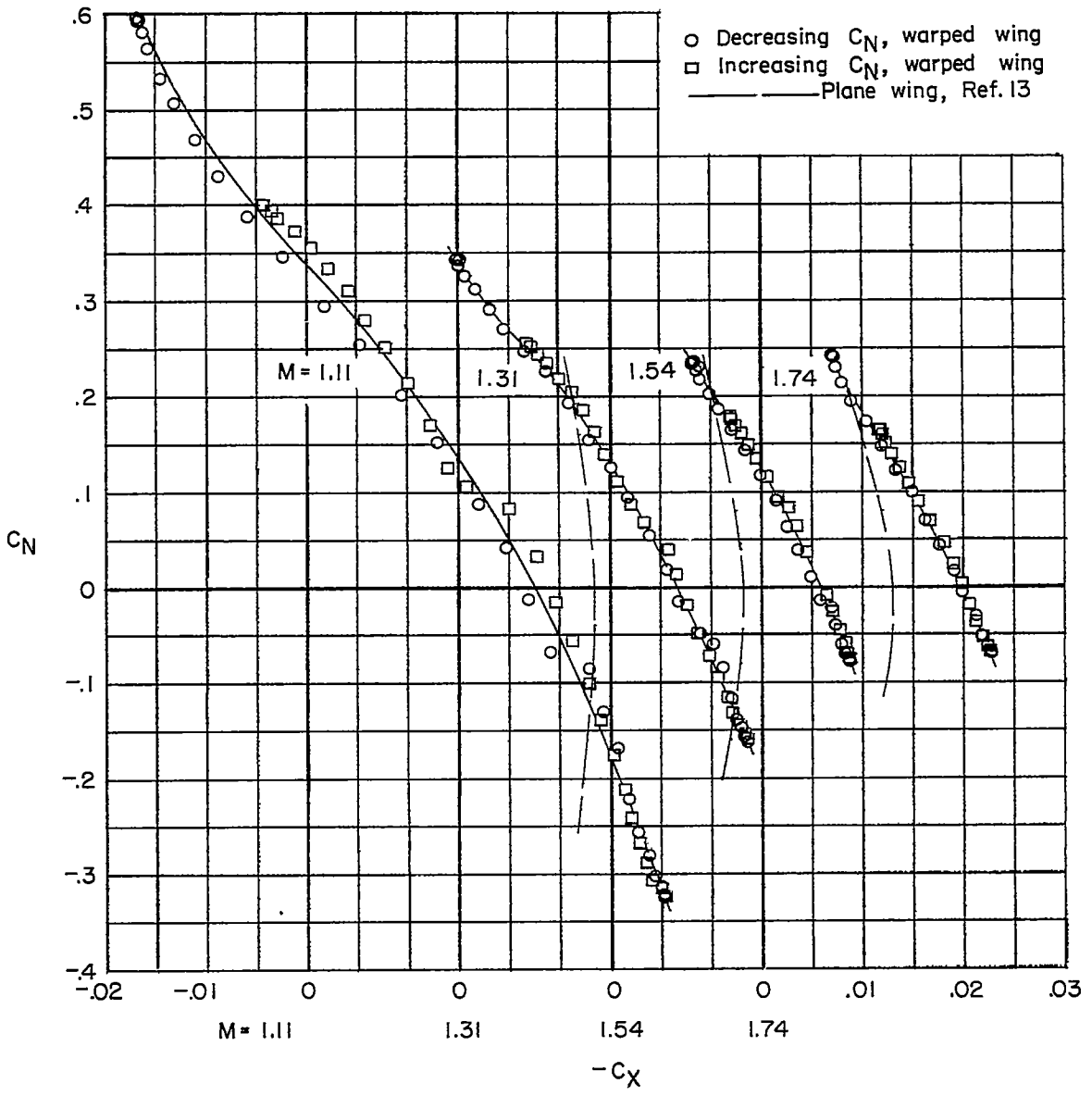

Figure 7.- Variation of normal-force coefficient with axial-force coefficient.

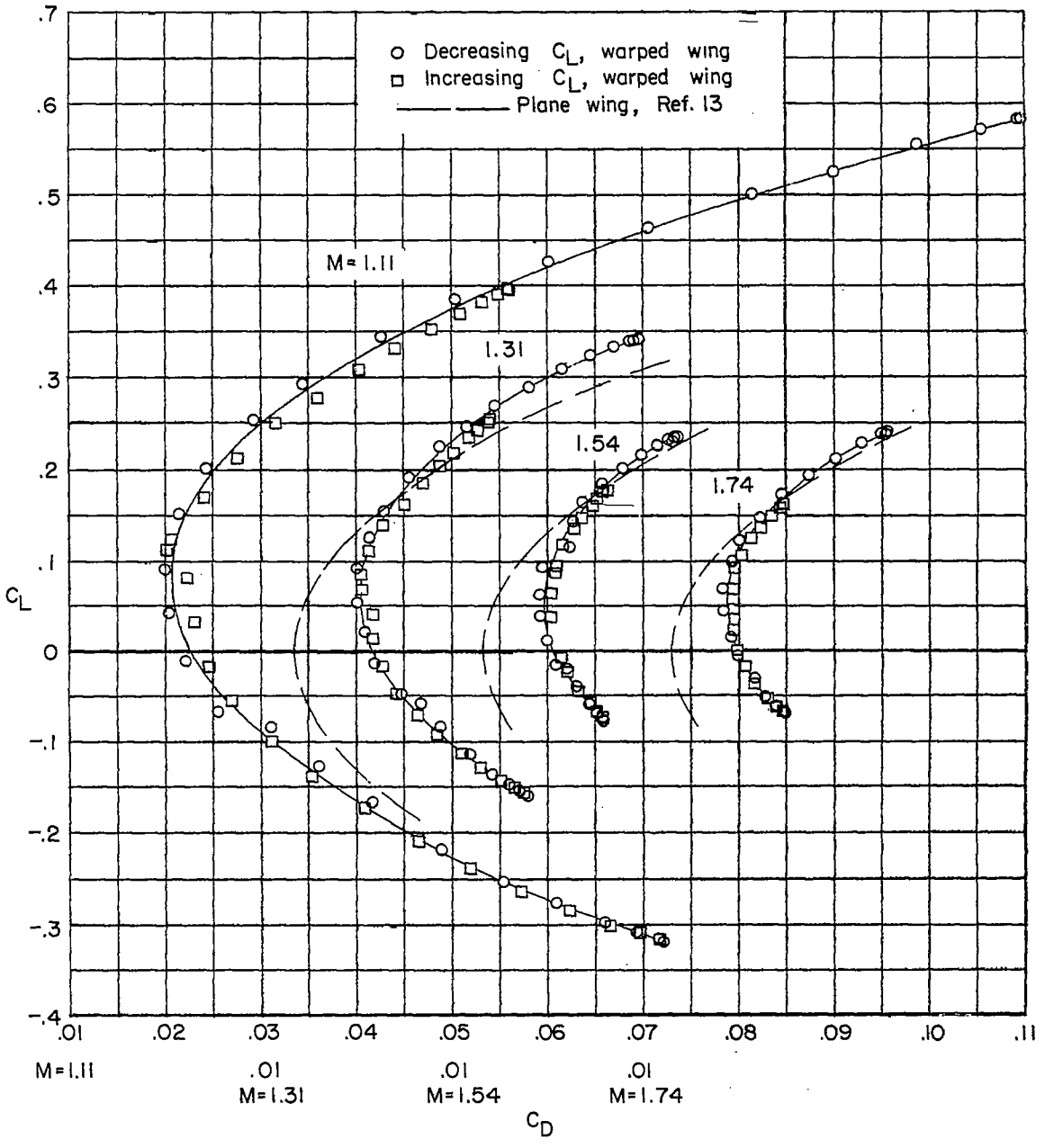

Figure 8.- Drag polars.

[redacted]

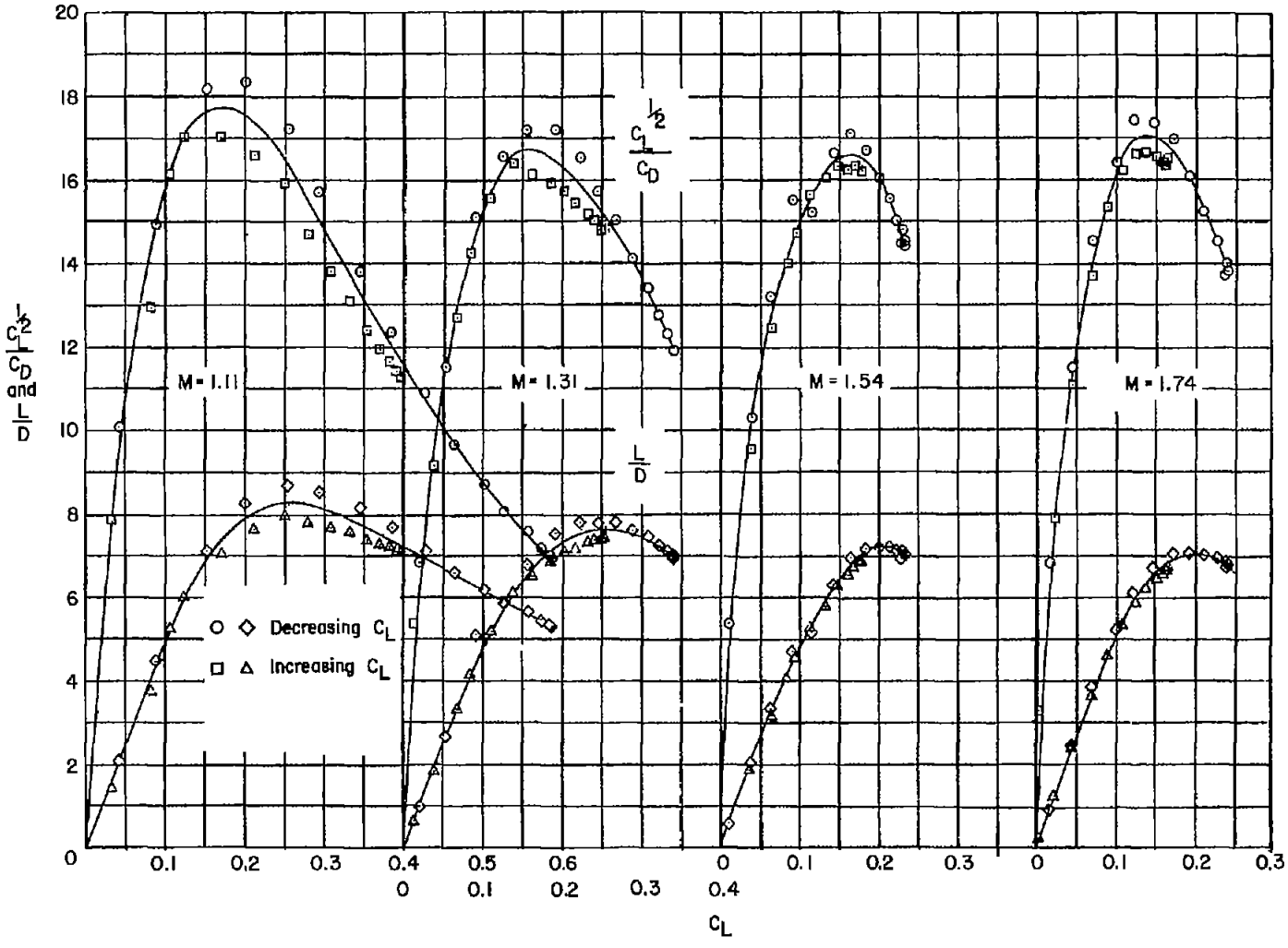

Figure 9.- Variation of L/D and $\frac{C_L^{1/2}}{C_D}$ with C_L.

[redacted]

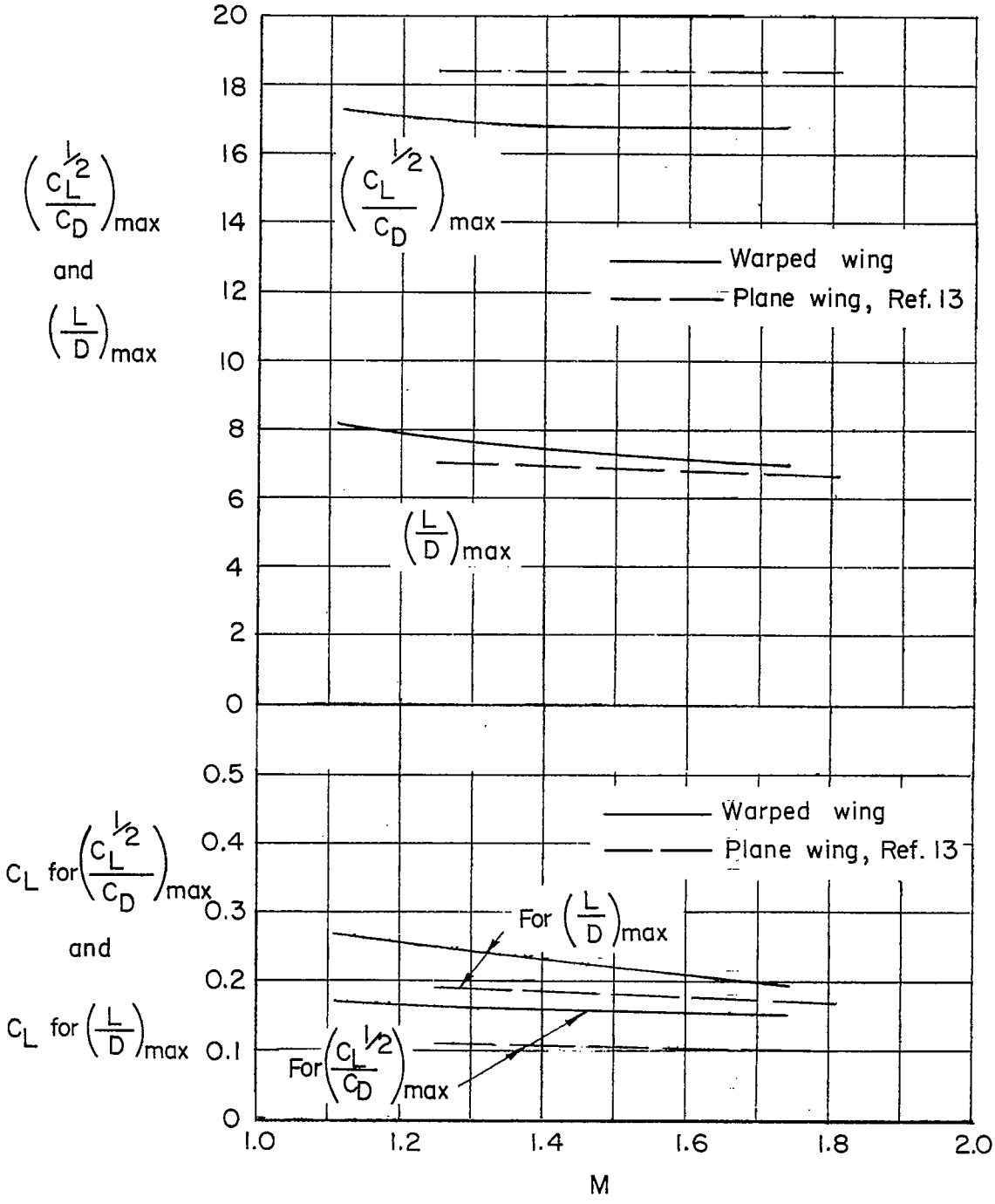

Figure 10.- Aerodynamic performance parameters and optimum lift coefficients.

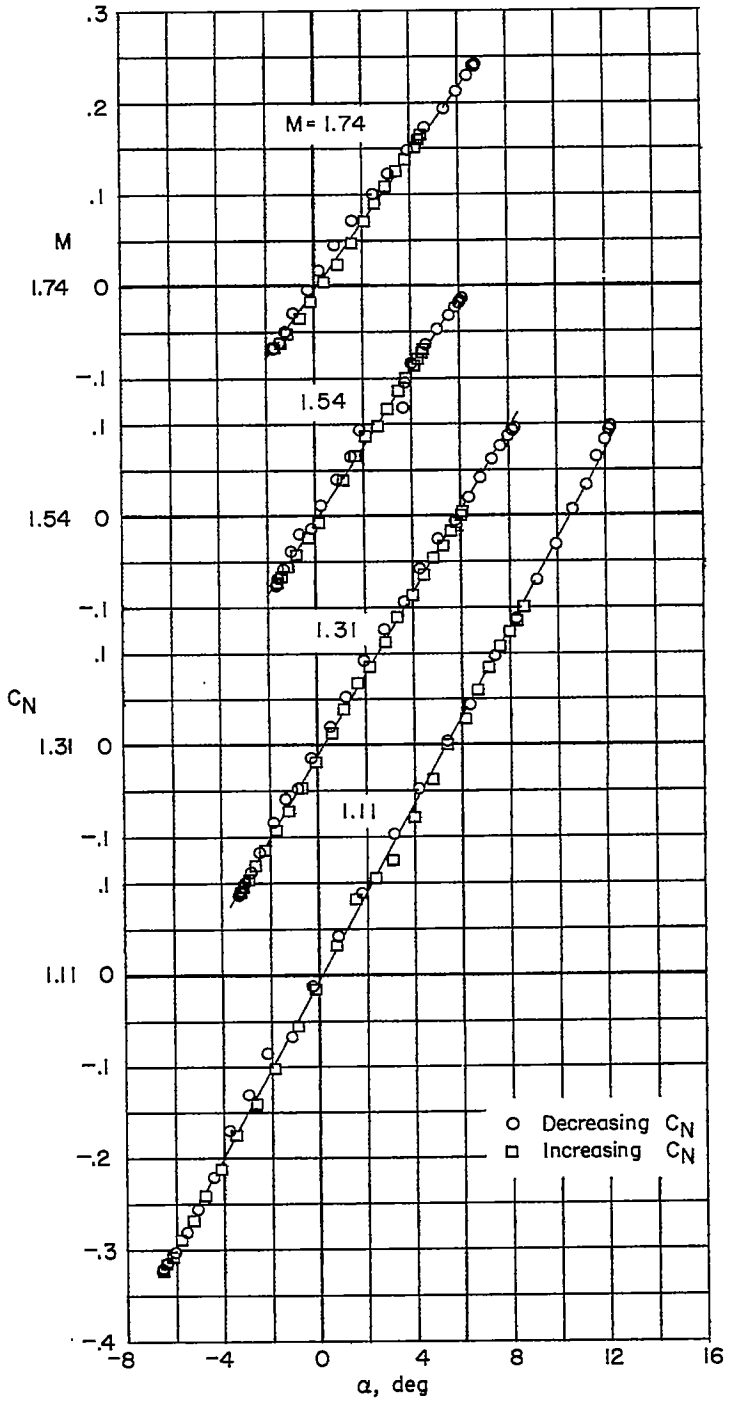

Figure 11.- Variation of normal-force coefficient with angle of attack.

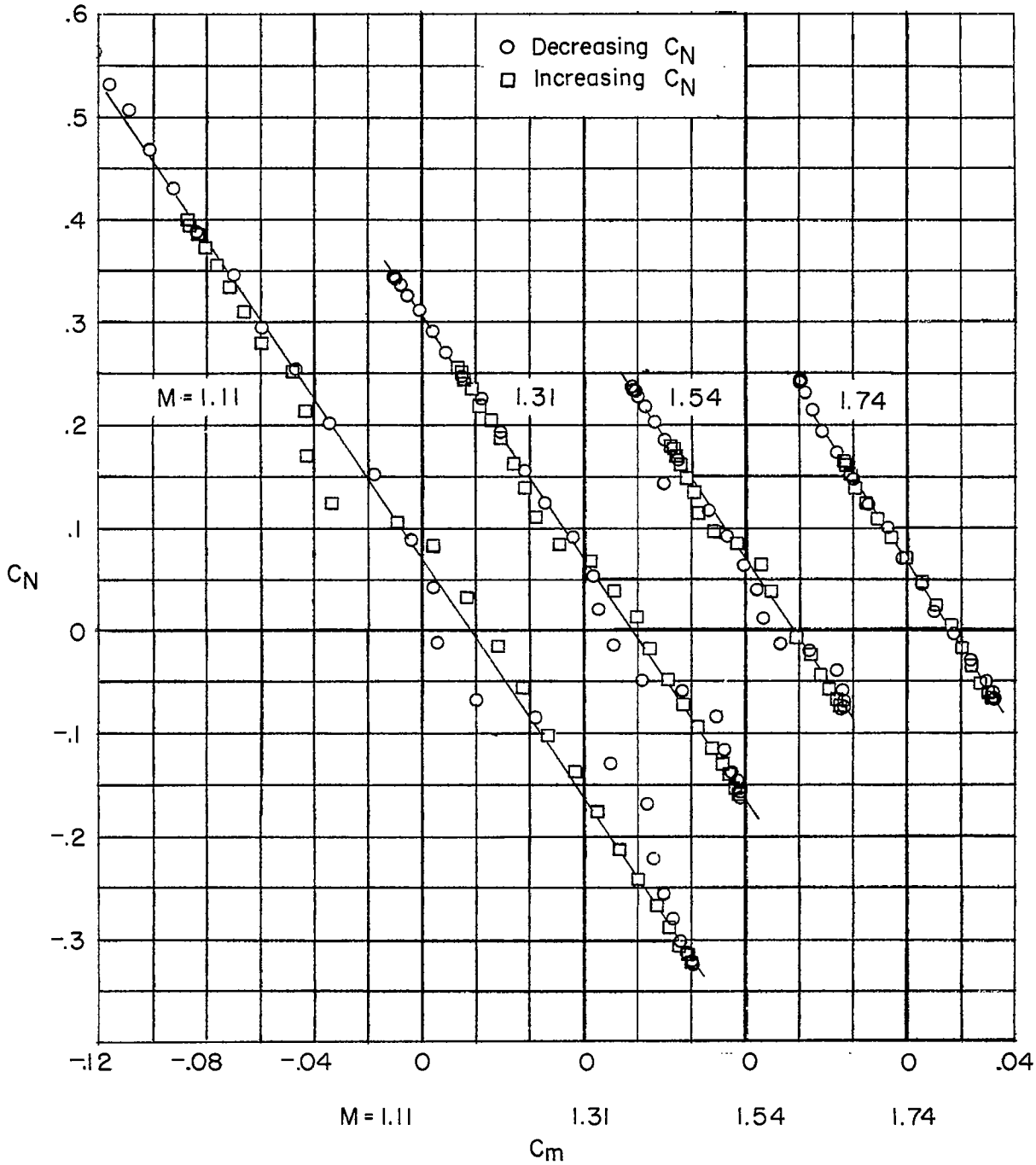

Figure 12.- Variation of normal-force coefficient with pitching-moment coefficient.

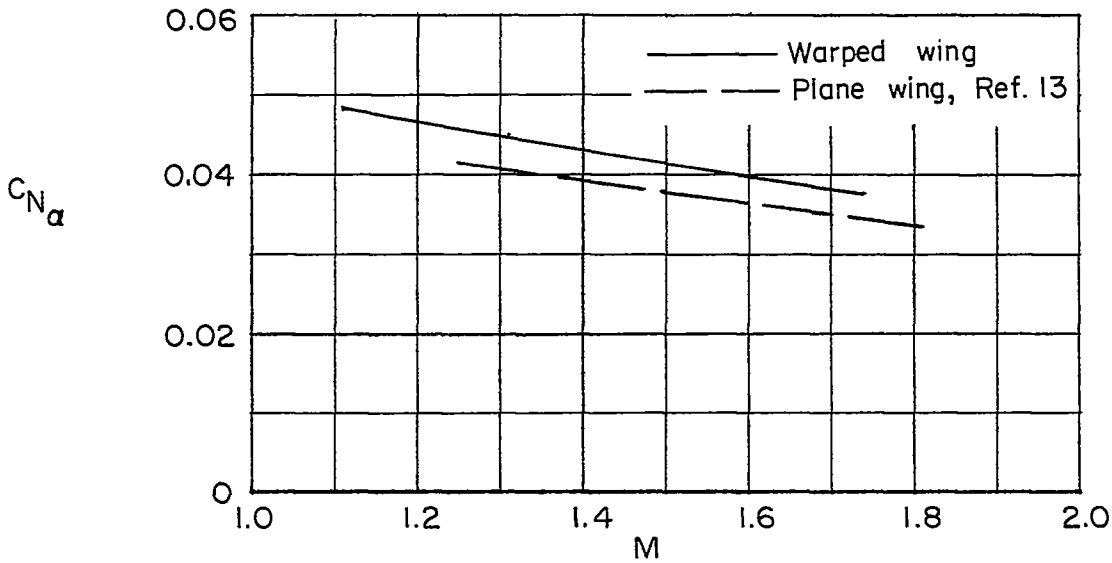

(a) Normal-force-curve slope C_{N_α}.

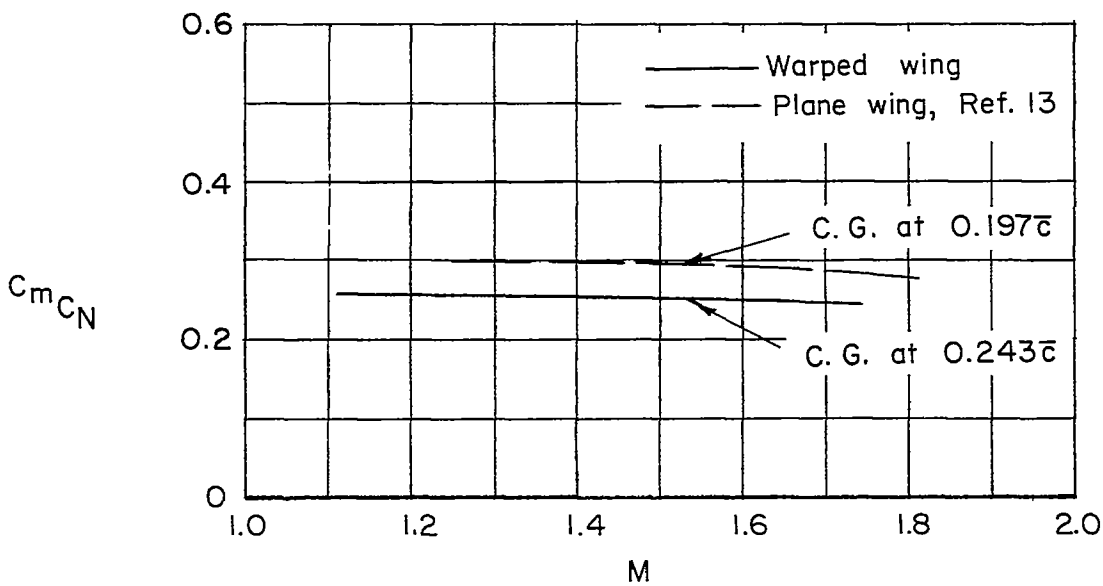

(b) Static-stability parameter $C_{m_{C_N}}$.

Figure 13.- Lift effectiveness and static stability parameters against Mach number.